High speed (>13 GHz) modulation of 850 nm vertical cavity surface emitting lasers (VCSELs) with tapered oxide confined layer

Y.H. Chang, H.C. Kuo, F.-I. Lai, K.F. Tzeng, H.C. Yu, C.P. Sung, H.P. Yang and S.C. Wang

Abstract: Improved oxide-implanted VCSELs utilising the tapered oxide layer are presented. The VCSELs exhibited similar static performance, but superior modulation bandwidth up to 13.2 GHz, compared with conventional blunt oxide VCSELs. The damping rate was reduced two times in the tapered oxide VCSEL and therefore enhanced the maximal modulation bandwidth. A very clean eye was demonstrated from the improved VCSEL with a rising time of 26 ps, falling time of 40 ps and jitter of less than 20 ps, operating at 10 Gbit/s with 6 mA bias and 6 dB extinction ratio. A comprehensive small signal measurement and analysis was conducted. Based on the equivalent circuit model, the extrinsic bandwidth limitation of the tapered oxide VCSELs was determined.

1 Introduction

850 nm oxide-confined vertical cavity surface emitting lasers (VCSELs) have become a standard technology for applications in local area networks (LANs) and storage area networks (SANs). The main advantages of VCSELs are low threshold current, low divergence angle, and circular beam, leading to simpler packaging and low electrical power consumption. The surface emission property of VCSELs also simplifies the 2- dimensional arrays and enables wafer level testing, thus low fabrication cost [1]. For optical communication applications, high modulation bandwidth is desirable. Principal factors affecting laser diode modulation bandwidth are the relaxation oscillation frequency, optical nonlinearities, and parasitic circuit effects. Spatial hole burning (SHB) was known as one of the limitations on the bandwidth of VCSELs by inhibiting high resonance frequencies [2, 3]. Owing to the nonuniform optical intensity, carriers at different locations in the quantum well have different stimulated recombination rates, and therefore exhibit different dynamic responses to small signal modulation. This nonuniformity causes an overdamping of the relaxation oscillation, and makes the intrinsic maximum bandwidth of oxide VCSELs much smaller than predicted by the conventional rate equation model, which assumes uniform optical intensity.

Tapered oxide layer were first introduced to reduce low scattering loss for small aperture VCSELs [4]. Recently, tapered oxide was investigated theoretically to reduce the nonlinear damping effect by making the electrical aperture smaller than the optical aperture, and thereby improving the modulation bandwidth [5]. Additionally, the tapered aperture also has lower parasitic capacitance. When devices are under modulation, the parasitic capacitance across a thin oxide layer ($\sim$ 30 nm) will limit the high speed performance [6]. A thicker oxide layer would help to reduce the capacitance. Unfortunately, thick oxide layers incur excess scattering losses. The tapered oxide can be thick at the boundary of a mesa to provide a lower capacitance without the expense of excess scattering losses.

We previously demonstrated a simple planar approach for high-speed oxide-implanted VCSELs with good static operation characteristics and reliability [7, 8]. In this paper, we present the improved VCSELs utilising a tapered oxide layer. The VCSELs exhibited similar static performance compared with the previous devices, but superior high speed performance. The improvement was attributed to the reduced damping rate in the tapered oxide VCSEL. The extrinsic bandwidth limitation of the tapered oxide VCSELs was determined based on the equivalent circuit model.

2 Experimental

The VCSEL epi-wafers were grown by Aixtron 2400 G3 metal-organic chemical vapor-phase deposition (MOCVD) on an n^+-GaAs substrate, the structure of which consists of three $GaAs/Al_{0.3}Ga_{0.7}As$ (80 Å/80 Å) quantum wells, sandwiched by fully doped n- and p-DBR mirrors. Both n- and p-DBRs are composed of interlaced $1/4\lambda$-thick $Al_{0.15}Ga_{0.85}As$ and $Al_{0.9}Ga_{0.1}As$ layers, with periods of 39.5 and 22, respectively. The gain peak position = 835 nm was determined by photoluminescence while the FP-dip wavelength = 845 nm was determined by reflection measurement. For blunt oxide VCSELs, a 30 nm-thick $Al_{0.98}Ga_{0.02}As$ layer was placed in node position. For tapered oxide VCSELs, the tapered oxide layer was formed by a 10 nm-thick $Al_{0.99}Ga_{0.01}$ layer adjacent to a 200 nm thick $Al_{0.98}Ga_{0.02}As$ layer, similar to [4]. The oxide-confined VCSEL process procedure has been described elsewhere [7, 8]. The mesa diameter of the fabricated device

© IEE, 2005

IEE Proceedings online no. 20045068

doi: 10.1049/ip-opt:20045068

Paper first received 6th December 2004 and in revised form 17th February 2005

Y.H. Chang, H.C. Kuo, F.-I. Lai, K.F. Tzeng and S.C. Wang are with the Department of Photonics and Institute of Electro-optical Engineering, National Chiao-Tung University, Hsin-Tsu 300, Taiwan, ROC

H.C. Yu, C.P. Sung and H.P. Yang are with the Opto-Electronics and System Laboratory, Industrial Technology Research Institute Hsin-Tsu 310, Taiwan, ROC

E-mail: nckno@faculty.nctu.edu.tw

was 30 μm with a 5.5 μm oxide aperture. The diameter of the oxide aperture was determined by dark-field microscopy and the size of the spontaneous emission pattern. The device surface was quasi-planar so that the annular p-contact metal and the bond pad were at the same level. The p-contact was created by directly depositing Ti/Pt/Au on the upper heavily-doped p^+ GaAs contact layer, and Au/Ge/Ni/Au was deposited on the bottom side of the substrate following thinning down. Multiple proton implantations with a dose in the range of $10^{13} \sim 10^{15}\,cm^{-2}$ and four different proton energy ranges between 200 to 420 keV were adapted according to simulation results of the stopping and range of ions in matter (SRIM). The implantation region was kept away from the mesa to prevent damage to the active region and consequent voiding of triggering reliability issues.

3 Results and discussion

The DC characteristics of completed VCSELs were measured with a probe station, an Agilent 4145A semiconductor parameter analyser and an NIST traceable integration sphere with a photodiode. Figure 1 plots curves of light output and voltage against current (LIV) of typical VCSELs for both tapered oxide VCSELs and blunt oxide VCSELs with 5.5 μm aperture. The threshold current is ~ 1 mA (0.9 mA) for tapered (blunt) type VCSELs with the same slope efficiency of ~ 0.35 mW/mA. The similar static performance is not surprising since the oxide apertures here have the same size of $5 \sim 6$ μm, and the blunt oxide does not incur excess scattering except at very small oxide size (< 3 μm). The maximal output power exceeds 3 mW at room temperature and output power rollover occurs as the current increases above 12 mA.

The small signal response of the VCSELs was measured using a calibrated vector network analyser (Agilent 8720ES) with wafer probing and a 9 μm optical fibre connected to a New Focus 40 GHz photodetector. The emission of the VCSEL was collimated and then focused to a diffraction-limited spot by a $10\times/20\times$ objective pair (NA = 0.25/0.4). The overall coupling efficiency is around $20 \sim 30\%$. Figures 2*a* and *b* show the modulation response of the VCSELs with the bias current for both tapered oxide VCSELs and blunt oxide VCSELs. At low bias currents, the bandwidth increased in proportion to the square root of the current above threshold, as expected from the rate equation analysis. For blunt oxide VCSELs, low frequency rollover was observed and the modulation response became gradually overdamped as the bias current

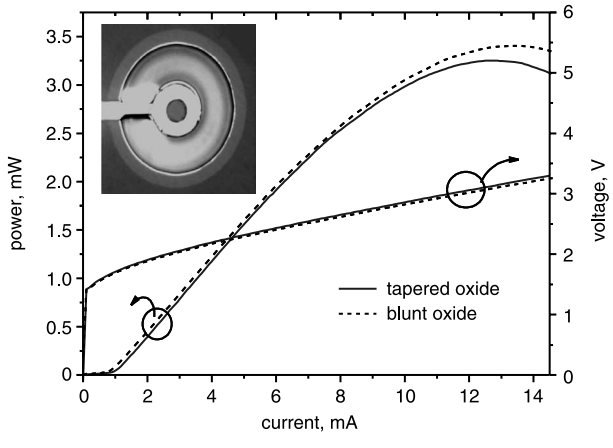

Fig. 1 *L-I-V curves of the tapered oxide and the blunt oxide VCSELs*
Inset: Top view image of the VCSEL

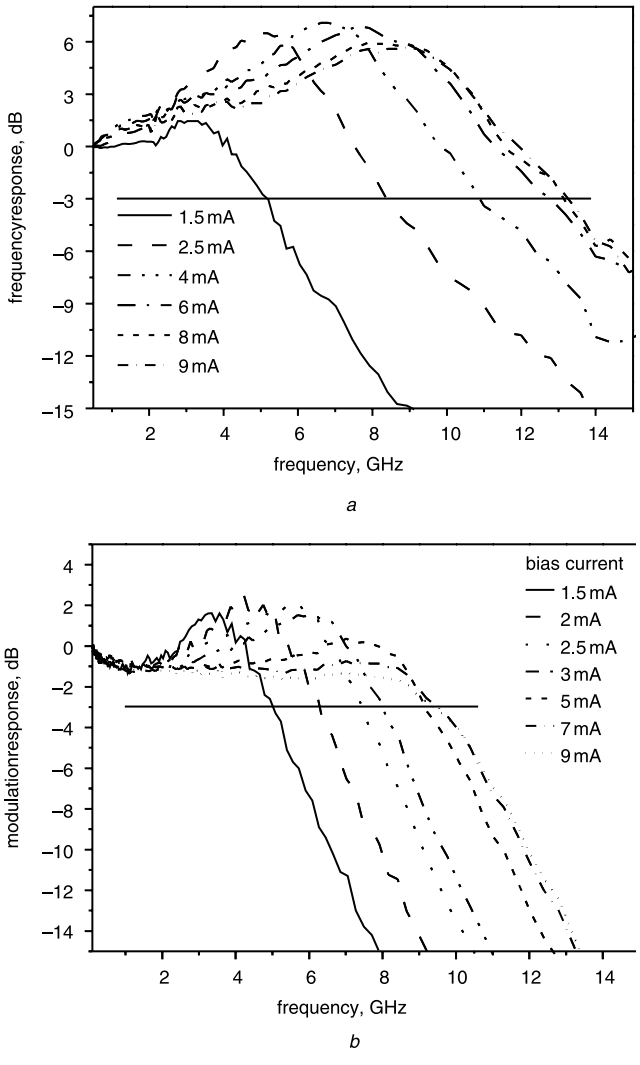

Fig. 2 *Small signal modulation responses*
a Tapered oxide VCSEL
b Blunt oxide VCSEL

increased. In contrast, no rollover was observed at low frequency for tapered oxide VCSELs and the 3 dB bandwidth reached a maximum value of 13 GHz before being fully overdamped. The observations coincide with the simulation results for blunt oxide VCSEL in which a

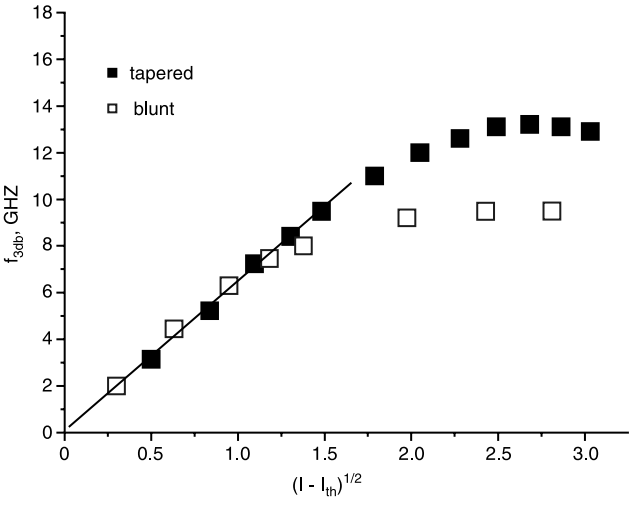

Fig. 3 *3 dB frequency of oxide-implanted VCSELs against root square of bias current above threshold*

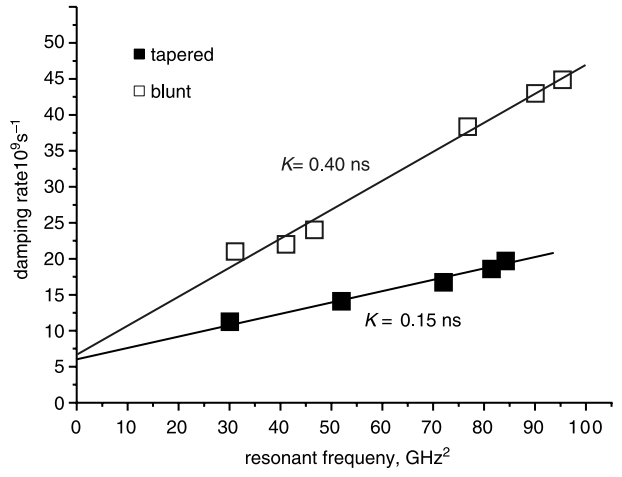

Fig. 4 *Damping rate against resonance frequency squared for VCSELs*

significant overdamping was reported in the relaxation oscillation owing to the nonuniformity of the transverse mode and significantly reduced the modulation bandwidth. [2, 5].

In Fig. 3, the 3 dB bandwidth is plotted with the root square of the bias current above threshold. The bandwidths are similar at low bias current for both tapered oxide VCSELs and blunt oxide VCSELs and saturated at the bias current higher than 8 mA. The maximal bandwidth for the blunt oxide VCSELs was 9.5 GHz and was enhanced to 13.2 GHz for the tapered oxide VCSELs. The modulation current efficiency factor was $\sim 6.5\,\mathrm{GHz}/(\mathrm{mA})^{1/2}$. As shown previously in Fig. 2, the peak height of modulation response was higher in the tapered oxide VCSEL than that of the blunt oxide VCSEL. The higher modulation amplitude in tapered oxide VCSELs implies a lower damping rate, which was known to be approximately proportional to the ratio between resonant frequency and peak modulation amplitude [9]. In depth, the damping rate, resonant frequency, and parasitic roll-off frequency can be obtained by fitting the experimental data to a three-pole approximation of the modulation response equation [9]. The K factor can be found from the slope of damping rate plotted against the square of resonant frequency, shown in Fig. 4. It was shown that the damping rate is indeed about two times higher than that in blunt oxide VCSELs and the K factors

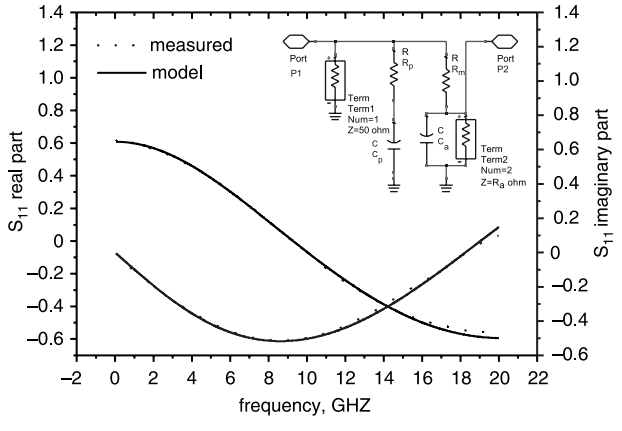

Fig. 5 *Real and imaginary parts of S_{11} parameter against frequency from model and measured data*

Inset: Equivalent circuit model of VCSELs

were 0.15 ns and 0.4 ns respectively. The comparison of the damping rate is also coincident with the theoretical prediction [2, 5]. If parasitic and other heating effects are ignored, the theoretical damping-limited 3 dB bandwidth may be over 59 GHz for a tapered oxide VCSEL and 22 GHz for a blunt oxide VCSEL, from the ratio of $2\pi(2)^{1/2}/K$ [9].

As previously shown in Fig. 2*a*, the 3 dB bandwidth reached a maximum value of $\sim$ 13 GHz before being fully overdamped. We therefore investigate the extrinsic bandwidth limitation on the tapered oxide VCSELs. An equivalent circuit for the VCSEL impedance is useful for analysis of electrical bandwidth limitations. The inset of Fig. 5 shows the equivalent circuit model used to extract the circuit components. The resistance Rm represents the mirror loss while Ra accounts for active region resistance. Ca represents a combination of capacitance of the active area and oxide layer. A shunt resistance Rp is also included to account for pad loss and the pad capacitance is represented by Cp. Using this equivalent circuit, we can investigate also the extrinsic limitations on the modulation speed and determine the influence of parasitic capacitance and mirror resistance on the modulation bandwidth. To extract the capacitance of the VCSELs, the measured amplitude and the phase of S_{11} data were fitted from 100 MHz to 20 GHz. Figure 5 illustrates measured and fitted S_{11} results for the tapered oxide VCSEL at 6 mA. Convergence of the fitting values to physically reasonable values was obtained using the following procedure. First, C_p, R_p, rmR_{rmm}, and rmC_{rma} were extracted using zero bias S_{11} data (where R_a is very large and can be neglected). Second, R_a and C_a values were extracted by fitting the S_{11} data for different bias currents. Finally, all the circuit parameters were allowed to vary about these values in order to minimise the squared error. The resulting C_p, R_p, and R_m were 160 fF, 5Ω and 51Ω respectively and the extracted R_a and C_a values for different bias currents are listed in Table 1. Based on these extracted values, the electrical bandwidth can be determined from -3 dB of the S_{21} of the equivalent circuit shown in the inset of Fig. 5. In consequence, an electrical bandwidth of $\sim$ 12.5 GHz was obtained and showed weak dependence on bias current. The calculated electrical bandwidth is coincident with the maximal measured modulation bandwidth and confirms the parasitic effects as the main limitation on the tapered oxide VCSELs.

Finally, the eye diagram of a tapered oxide VCSEL was demonstrated. Microwave and lightwave probes were used in conjunction with a 10 Gbit/s pattern generator (MP1763 Anritsu) with a pseudorandom bit sequence of $2^{31}-1$ and a 12.5 GHz photoreceiver. Eye diagrams were obtained for back-to-back (BTB) transmission on VCSELs via a multimode fibre. Figure 6 shows the room temperature eye diagram of the tapered oxide VCSEL with compliance OC-192 mask. The eye diagram was measured at 6 mA with an extinction ratio of 6 dB. The clear open eye pattern indicates good performance of these VCSELs with the rising time (T_r) of 26 ps, the falling time (T_f) of 40 ps, and jitter $(p-p) < 20$ ps.

Table 1: Extracted circuit values at different bias currents for tapered oxide VCSELs

Bias (mA)	0	1	2.5	4	6	8	10
$R_a(\Omega)$	∞	200	162	136	113	96	87
$C_a(fF)$	185	191	197	202	210	221	240

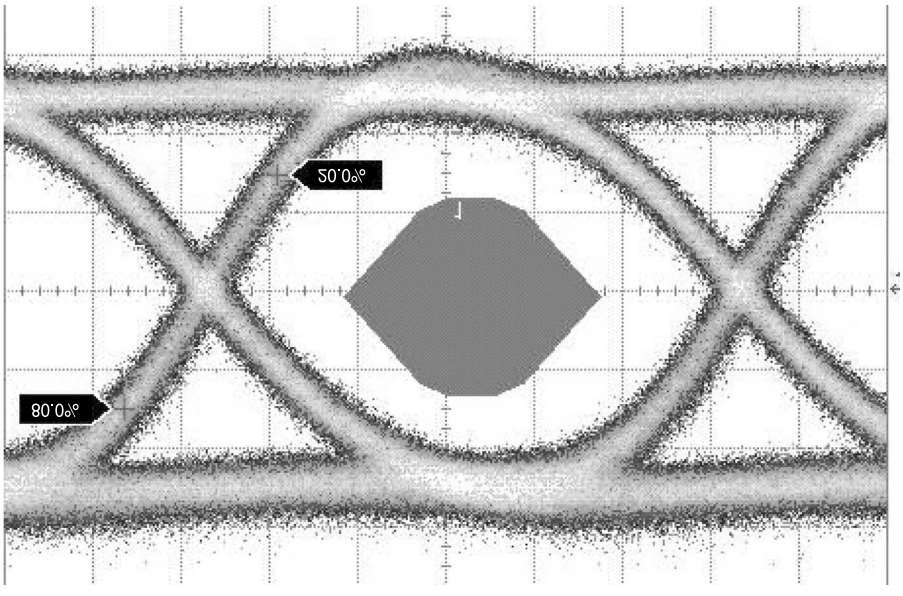

Fig. 6 *Eye diagram of tapered oxide VCSEL at PRBS of $2^{31} - 1$ and 6 dB extinction ratio, biased at 6 mA*
Time scale is 15.6 ps/div

4 Conclusion

Planarised oxide-implanted VCSELs were fabricated utilising tapered oxide layer. The VCSELs exhibited similar static performance, but superior modulation bandwidth up to 13 GHz, compared with VCSELs utilising a conventional blunt oxide layer. A very clean eye diagram was demonstrated with rising time of 26 ps, falling time of 40 ps and jitter of less than 20 ps operating at 10 Gbit/s with 6 mA bias and 6 dB extinction ratio. The devices are fabricated using a simple, reliable planarised process and can be suitable for mass production. The high bandwidth and good eye characteristics make these devices very promising in future 10 Gbit/s or even higher modulation applications.

5 Acknowledgments

The authors would like to thank the National Science Council, Republic of China (ROC), (Contract No. NSC-90-2215 -E009-088) and the Academic Excellence Program of the Ministry of Education of the ROC (Contract No. 88-FA06-AB) for financially supporting this research. Dr. C.P. Kuo of LuxNet Corporation and Dr I- Tsing Tan of JDSU Corporation are appreciated for their valuable insights and Mrs. J. M. Wang of ITRI for providing technical support. The Institute of Nuclear Energy is also appreciated for supporting the proton implantation under Contract No. 922001InER015

6 References

1 Aeby, I., Collins, D., Gibson, B., Helms, C.J., Hou, H.Q., Luo, W., Bossert, D.J., Wang, C.X., Photonic West, San Jose, CA, USA, 2003, **4994**, pp. 152–161
2 Valle, A., Sarma, J., and Shore, K.A.: 'Spatial hole burning effects on the dynamics of vertical cavity surface-emitting laser diodes', *IEEE J. Quantum Electron.*, 1995, **31**, pp. 1423–1431
3 Liu, Y., Ng, W.-C., Oyafuso, F., Klein, and Hess, K.: 'Simulating the modulation response of VCSELs: the effects of diffusion capacitance and spatialhole-burning', *IEE Proc. Optoelectron.*, 2002, **149**, pp. 182–188
4 Hegblom, E.R., Thibeault, B.J., Naone, R.L., and Coldren, L.A.: 'Vertical cavity lasers with tapered oxide apertures for low scattering loss', *Electron. Lett.*, 1997, **33**, pp. 869–879
5 Liu, Y., Ng, W.-C., Klein, B., Hess, K., *IEEE J. Quantum Electron.*, 2003, **39**, pp. 99–108
6 Chang, C.H., Chrostowski, L., and Chang-Hasnain, C.J.: 'Parasitics and design considerations on oxide-implant VCSELs', *IEEE Photon. Technol. Lett.*, 2001, **13**, p. 1274
7 Yu, H.C., Chang, S.J., Su, Y.K., Sung, C.P., Lin, Y.W., Yang, H.P., Huang, C.Y., and Wang, J.M., *Mater. Sci. Eng. B.*, 2004, **106**, pp. 101–104
8 Chang, Y.H., Lai, F.-I., Lu, C.Y., Kuo, H.C., Yu, H.C., Sung, C.P., Yang, H.P., and Wang, S.C., *Semicond. Sci. Technol.*, 2004, **19**, pp. L74–L77
9 Agrawal, G.P., and Dutta, N.K.: 'Semiconductor lasers', 2nd edition (Van Nostrand Reinhold), pp. 276–280